External ring-cavity quantum cascade lasers

Cite as: Appl. Phys. Lett. **102**, 141105 (2013); https://doi.org/10.1063/1.4800073
Submitted: 07 January 2013 . Accepted: 22 March 2013 . Published Online: 10 April 2013

Pietro Malara, Romain Blanchard, Tobias S. Mansuripur, Aleksander K. Wojcik, Alexey Belyanin, Kazuue Fujita, Tadataka Edamura, Shinichi Furuta, Masamichi Yamanishi, Paolo de Natale, and Federico Capasso

External ring-cavity quantum cascade lasers

Pietro Malara,[1,2] Romain Blanchard,[1] Tobias S. Mansuripur,[3] Aleksander K. Wojcik,[4] Alexey Belyanin,[4] Kazuue Fujita,[5] Tadataka Edamura,[5] Shinichi Furuta,[5] Masamichi Yamanishi,[5] Paolo de Natale,[2] and Federico Capasso[1]
[1]*School of Engineering and Applied Sciences, Harvard University, Cambridge, Massachusetts 02138, USA*
[2]*Consiglio Nazionale delle Ricerche–Istituto Nazionale di Ottica and European Laboratory for Nonlinear Spectroscopy (LENS), 80078 Pozzuoli (NA), Italy*
[3]*Department of Physics, Harvard University, Cambridge, Massachusetts 02138, USA*
[4]*Department of Physics and Astronomy, Texas A&M University, College Station, Texas 7784, USA*
[5]*Central Research Laboratory, Hamamatsu Photonics K. K., Hamamatsu 434-8601, Japan*

(Received 7 January 2013; accepted 22 March 2013; published online 10 April 2013)

An external ring-cavity quantum cascade laser (QCL) is demonstrated. Gain competition between the clockwise and anticlockwise ring-cavity modes results in a transition from bidirectional to directional emission as current is increased. In the directional regime, spatial hole burning (SHB) is suppressed, and the spectrum evolves to a single longitudinal mode, in contrast with the multimode spectrum of a comparable Fabry-Pérot QCL. The absence of SHB and the long path-length of the external cavity make this laser an excellent candidate for active mode-locking and high-sensitivity spectroscopic applications in the mid-infrared. A proof-of-principle intracavity absorption spectroscopic detection of water vapor is demonstrated. © *2013 American Institute of Physics*.
[http://dx.doi.org/10.1063/1.4800073]

The standing wave pattern formed by counter-propagating waves in a Fabry-Pérot (FP) laser cavity imprints a half-wavelength period grating in the gain medium through gain saturation. Such a spatially inhomogeneous distribution of the gain, known as spatial hole burning (SHB), plays an important role in the temporal and spectral dynamics of many lasers. In quantum cascade lasers (QCLs) SHB effects are particularly pronounced because the gain recovery time is faster than the carrier diffusion time, so the gain saturation grating cannot be washed out by carrier diffusion.[1] For example, multimode emission of FP-QCLs can result from SHB: new modes can reach the lasing threshold as they experience gain in the nodes of a grating imprinted by another lasing mode.

It has also been demonstrated that SHB is a fundamental limitation for active mode-locking of monolithic QCLs[2] since it competes with the mode-locking process (e.g., active gain modulation) to impose a particular phase relationship between longitudinal modes. This leads to strongly structured pulses and eventually destabilizes mode-locking as soon as the pumping current is pushed slightly above threshold. It has been shown that this limitation on the stable mode-locking operating range prevents the formation of pulses with energies high enough for any practical application.[3]

Traveling wave resonators such as ring cavities support both clockwise (CW) and counterclockwise (CCW) traveling modes which are not inherently coupled through facet reflections. Therefore, SHB will be suppressed in a ring cavity in the following two situations: (1) only one of the modes (either CW or CCW) lases or (2) both modes lase simultaneously but in the absence of any mechanism which could couple the two modes and lock their relative phase, so that the drifting phases of the modes effectively wash out the standing wave. In practical setups, however, small spurious reflections from cavity elements will lock the relative phase of the CW and CCW modes.[4] Therefore, unidirectional operation is required to suppress SHB.

With visible and telecom wavelength ring lasers unidirectional operation can be achieved by incorporating a non-reciprocal optical element, such as an optical isolator, in the cavity. In the mid-infrared (mid-IR), where these devices are not yet well-established, one reported effort to achieve directional emission of a monolithic ring QCL was to incorporate an S-shaped cross-over branch within a racetrack cavity in order to convert some of the CW mode into the CCW mode.[5] This asymmetry led to directional emission with a counter-propagating wave suppression ratio (CWSR) of 9. To our knowledge, no further investigations were performed.

Interesting current-dependent CW/CCW mode competition effects have been demonstrated in monolithic diode ring lasers (SRLs) when a loss imbalance between the CW and CCW modes is not intentionally implemented.[6–9] Typically, a bidirectional regime at low current and a bistable unidirectional regime at large current are seen, with temporal oscillations of the modal power distribution at intermediate current levels. Such rich phenomena have been explained by models which include backscattering from chip imperfections and self/cross-gain saturation.[10,11]

In this work we investigate the modal dynamics of a ring laser formed by placing a mid-IR quantum cascade (QC) gain medium within a free-space-coupled external ring cavity (ERC). The effects of the ring cavity geometry are elucidated by directly comparing the power output and spectral characteristics of the ERC-QCL with a FP-QCL having the same gain medium.

The QC gain medium used in the experiments operates around 1250 cm^{-1} (Ref. 12) and was processed into a buried heterostructure waveguide 3 mm-long and 13 μm-wide. The waveguide was mounted epi-side up on a copper heat sink and held at 293 K by a thermoelectric cooler. The laser was first characterized as a FP-QCL, after which both facets were anti-reflection (AR) coated (using a bilayer of ZnSe and YF_3 (Ref. 13)), and the chip was then placed inside the ring

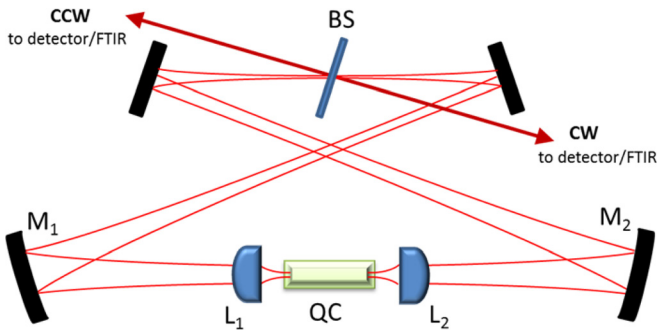

FIG. 1. External ring cavity QCL setup: radiation in the clockwise (counter-clockwise) direction is emitted from the left (right) facet of the QC gain medium, collimated by the lens L1 (L2), refocused by the spherical mirror M1 (M2) followed by M2 (M1), and re-injected into the QC gain medium waveguide by the lens L2 (L1). The total path length is 1.7 m. Out-coupling of both modes is provided by the beam splitter BS.

cavity to form the ERC-QCL, as sketched in Fig. 1. The radiation emitted from each waveguide facet was collimated by an aspheric chalcogenide glass lens with a numerical aperture of 0.852, positioned in front of the facet by a translation stage. The ERC was arranged in a bow-tie configuration with two spherical mirrors (0.5 m radius) and two flat mirrors, all with a nominal reflectivity of $R_{mir} = 0.96$. The total cavity length was $L_{cav} = 1.7$ m, yielding a roundtrip time of 5.7 ns and a corresponding free spectral range (FSR) of 176 MHz. The two counter-propagating modes of the ring cavity were out-coupled by means of a beam splitter (BS) with a nominal transmissivity of 0.45 at $\lambda = 8\,\mu$m, which could be slightly tuned by adjusting the angle of incidence. The out-coupled light was detected by two calibrated power meters or directed to a Fourier transform infrared (FTIR) spectrometer with 0.2 cm^{-1} resolution. In the following we will refer to the CW (CCW) mode as the one emitted from the left (right) facet, as illustrated in Fig. 1.

In Fig. 2, pulsed light-current (L-I) curves for the CW (black) and CCW (red) modes are plotted alongside the L-I

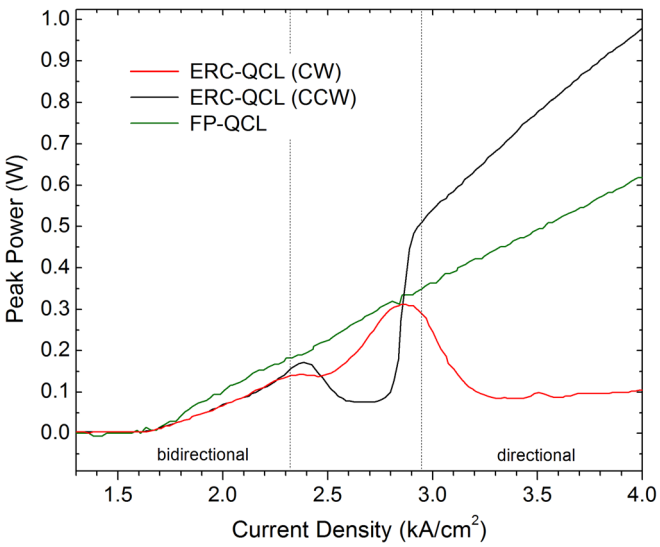

FIG. 2. Pulsed (1 μs width, 50 kHz repetition rate) L-I curves for the CW (red) and CCW (black) modes of the ERC-QCL, and for the single-facet emission of the FP-QCL (green). The vertical dotted lines separate the different regimes of the ERC-QCL as discussed.

of the FP-QCL (green). For the FP-QCL, the threshold current is 0.64 A, and the slope efficiency per facet is $(dP/dI)_{FP} = 0.69$ W/A. The ERC-QCL has a more complicated behavior, with two different L-I characteristics for the CW and CCW modes exhibiting a low-current regime with bidirectional emission, a high-current directional regime, and more complicated behavior at intermediate currents.

The threshold currents I_{th} for the CW and CCW modes are equal, and, for ease of comparing the two devices, the BS transmissivity was adjusted so that the ERC-QCL threshold was equal to the FP-QCL threshold. Due to this equality the single-pass gain at threshold of the two lasers is equal, which means that the round-trip losses of the ring cavity must equal the half-round-trip losses of the FP cavity. The waveguide loss of both lasers being equal, this condition becomes (assuming perfect AR coatings)

$$R_{facet} = R_{mir}^4 T_{BS} T_{in-coupl}, \tag{1}$$

where R_{facet} (=0.27) is the reflectivity of the uncoated FP facet, T_{BS} is the transmissivity of the beam splitter, and $T_{in\text{-}coupl}$ is the in-coupling efficiency from the external cavity into the QC waveguide.

At low currents the CW and CCW modes share the total emitted power equally and have the same slope efficiency $(dP/dI)_{ERC} = 0.49$ W/A; comparing this value to the slope efficiency of the FP-QCL using

$$\frac{\left(\frac{dP}{dI}\right)_{ERC}}{\left(\frac{dP}{dI}\right)_{FP}} = \frac{\ln(T_{BS})}{\ln(R_{facet})} \tag{2}$$

allows us to estimate $T_{BS} = 0.40$, and using Eq. (1) we find $T_{in\text{-}coupl} = 0.80$. When the pumping current exceeds 2.3 kA/cm^2, the total optical power is no longer shared equally between the CW and CCW modes. Instead, there are current-dependent fluctuations in the modal intensities, and either mode can be more intense depending on the current (Note: the reported L values indicate the time averaged power in each mode as seen by the power meter. When detecting the light with MCT detectors, scope traces (not shown) also demonstrate temporal oscillations of the shared optical power fraction at a fixed current as seen in some SRLs.[8]).

The fluctuations cease when the pumping current exceeds 3.25 kA/cm^2. Above this current, a directional regime is reached in which the optical power is concentrated almost entirely in one direction. In Fig. 2, the CCW mode is about 10 times more intense than the CW mode at the maximum current attainable with our pulse generator. Furthermore, the slope efficiency of the CCW mode is 1.11 W/A, ~2.3 times greater than the slope efficiency in the bidirectional regime (which is consistent with the notion that all the gain is used up by only one mode). We emphasize that the mode which dominates at high-current is determined by a small loss asymmetry between the CW and CCW modes; as such, we found that small adjustments to the alignment of the cavity could select one mode instead of the other to lase in the directional regime.

To understand how a loss imbalance in the ERC affects the lasing dynamics, we performed simulations based on the set of Maxwell-Bloch equations similar to Eqs. (12)–(15) in Ref. 3 and Eqs. (7)–(10) in Ref. 1. The Maxwell-Bloch equations correctly take into account the dynamics of optical coherence in the gain medium and the time-dependent effects of the optical saturation by the strong laser field. Let us define z to be the distance coordinate along the propagation direction, with $z=0$ at the left facet and z increasing in the clockwise direction. The total cavity length is $L_{cav}=L_g+L_{ext}$, where L_g is the length of the QC waveguide and L_{ext} is the length of the free-space portion of the cavity. In the ideal case where the QC waveguide has perfect AR coatings, we can express the CW field just after it enters through the right facet in terms of the field value just before exiting the left facet as $E_{CW}(L_{ext}^{+},t)=(1-\gamma_{CW})E_{CW}\left(0^{-},t-\frac{L_{ext}}{c}\right)$, where γ_{CW} is the total loss accumulated around the ERC in addition to the in-coupling loss. A similar condition holds for the CCW mode with a generally different loss parameter γ_{CCW}. We generalize this approach to also account for non-zero facet reflection coefficients which reflect part of the CW mode into the CCW mode and vice versa. In the simulation, we assume equal facet reflectivities $|r_{1,2}|^2=0.04$ and impose a small loss imbalance by choosing $\gamma_{CW}=0.5$ and $\gamma_{CCW}=0.505$. Initial conditions for the complex field amplitudes in the two directions were random noise, corresponding to spontaneous emission into laser modes. The resulting L-I curves of the two modes are shown in Fig. 3, which were generated by running the simulation multiple times for each current value and averaging over the resultant pulse intensities. The simulation predicts a bidirectional regime for currents up to 1.3 times the threshold, followed by a directional regime in which the mode with the smaller loss (CW, in this case) dominates as a result of gain competition. Another simulation (not shown) using zero facet reflectivities yielded only a directional regime beginning immediately after the threshold current. Thus, we can explain the bidirectional and directional regimes seen in the experiment as the result of a loss imbalance for the CW and CCW modes on the order of 1%, in addition to small residual facet reflectivities. To explain the experimental behavior at intermediate currents requires current-dependent losses which the simulation does not take into account. In the remainder of the paper we focus our attention on the directional regime, in which SHB is suppressed.

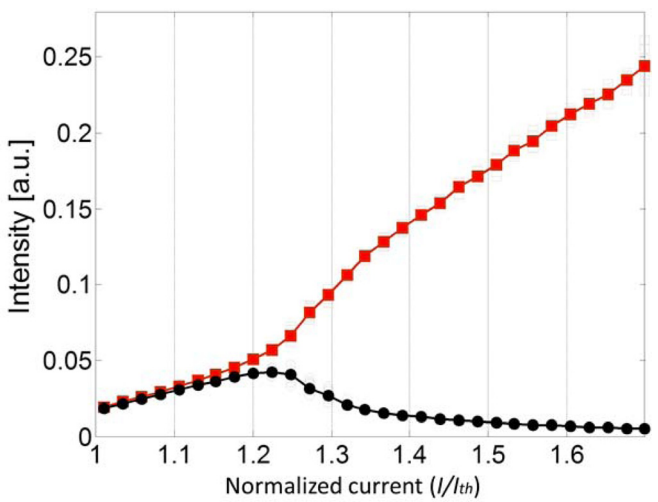

FIG. 3. Simulated L-I curves for the CW (red) and CCW (black) modes as a function of the normalized current I/I_{th}, calculated for the parameters specified. The curves are obtained by averaging over 10 electrical pulses for each value of the current.

To understand how the suppression of SHB in the directional regime affects the laser emission, spectra recorded with the FTIR spectrometer of both the FP and ERC-QCL are shown in Fig. 4. Because of the different cavity roundtrip times (0.06 ns and 5.7 ns for the FP- and ER-QCL, respectively) the spectral evolution of the ERC-QCL takes place on a longer timescale than the FP-QCL. In order to make a meaningful comparison, we recorded spectra for different pulse durations which corresponded to the same number of roundtrips in the two cavities. In these measurements the current was twice the threshold current for both lasers.

For pulse lengths on the order of hundreds of roundtrips, when the competition between longitudinal modes has not yet shaped the spectrum, the two lasers exhibit a similar broadband distribution of modes. As the pulse duration is increased, the FP-QCL reaches a spectral steady-state (after 10^4 roundtrips) characterized by a broad, structured multimode profile, which is commonly observed in FP-QCLs.[1] The ERC-QCL exhibits instead a narrowing of the average spectrum as the pulse length is increased. For 1 ms pulses (maximum length allowed by our pulser, which corresponds to 2×10^5 loops in the ring cavity), a single-mode spectrum with 10 dB side-mode suppression ratio (SMSR) is observed. We note that for spectral evolution measurements one would prefer time resolved spectra which show the instantaneous lasing spectrum at a given time, but this was not possible with our current setup. Instead, the reported spectra are averages over the full length of the pulse; one consequence of this is that the SMSR of the instantaneous spectrum of ERC-QCL radiation after 2×10^5 roundtrips is greater than the value measured here. The spectral narrowing to a single mode clearly shows that when SHB is effectively suppressed, there is no mechanism which supports multimode operation in this laser. Gain competition among the allowed longitudinal modes in the absence of a gain grating leads to a single-mode steady-state spectrum. These results represent a definite proof that the gain spectrum of this QCL active region is homogeneously broadened.

The presence of an external intracavity path and the reduced FSR make the ERC-QCL suitable for spectroscopic applications. A few detection techniques where a cavity with both absorption and gain is injected by an external laser have been successfully demonstrated in the near-infrared telecom region.[14,15] Also, the relatively slow spectral evolution and the possibility of directional operation of the ERC-QCL are particularly favorable for intracavity laser absorption spectroscopy (ICLAS), where information on the absorption within the laser cavity is retrieved from the transient laser spectrum.[16] To demonstrate the potential of this laser for ICLAS, we show in Fig. 5 ambient-air water vapor absorption lines burnt in the transient spectra of the ERC-QCL (recorded for three different central wavelengths achieved by varying the cavity alignment and heat sink temperature). A significant enhancement of the line contrast is seen when

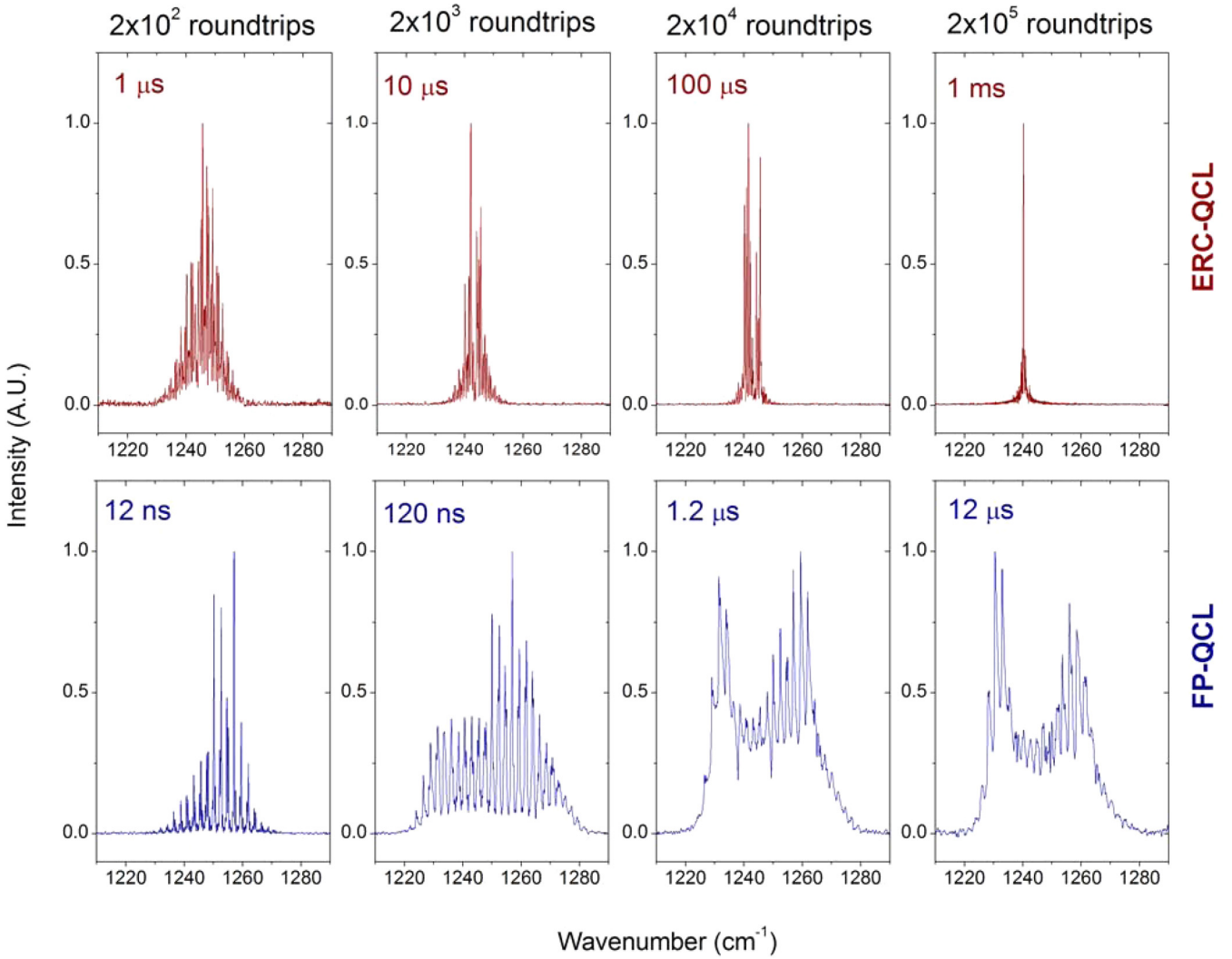

FIG. 4. Lasing spectra (averaged over the length of the pulse) of the ERC-QCL in the directional regime (red) and of the FP-QCL (blue), taken at pumping currents equal to twice the respective thresholds, for different pulse widths corresponding to the same number of roundtrips in the two cavities. For pulse widths of 1 ms (approximately 2×10^5 round trips) the ERC-QCL approaches single mode operation with an SMSR of 10 dB. The fringes observed in the ERC-QCL spectra for the three shorter pulse widths result from imperfect AR coatings on the collimating lenses ($R \sim 1\%$).

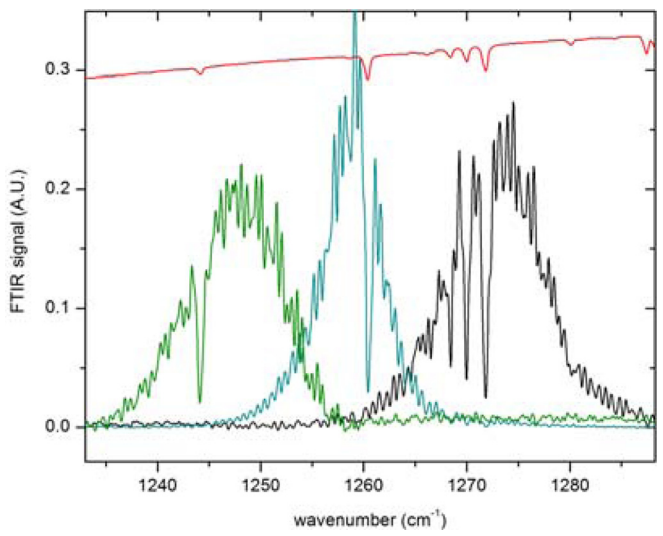

FIG. 5. Spectra of the ERC-QCL (pulse width = 30 μs, repetition rate = 2 kHz) at three different heat sink temperatures and alignment conditions (green, blue, brown). Cavity-enhancement of the ambient water-vapor absorption lines can be seen by comparison with the absorption spectrum taken with the FTIR globar source (red), demonstrating the potential of this laser for ICLAS.

compared to the ~1.2 m path length absorption spectrum taken with the FTIR's internal globar source (shown in red in Fig. 5), although this experiment is not sufficient to quantify it. The fringes in the laser spectra are the result of residual etalon structures in the laser, stemming from imperfect AR coatings of the collimating lenses and the QC waveguide facets, which need to be eliminated to effectively implement this technique.

The ERC-QCL also serves as a potentially useful platform for mode-locking a QCL to generate short mid-IR pulses. First, the elimination of SHB circumvents the instabilities which have hindered past attempts at mode-locking in FP-QCLs.[1–3] Second, the very small transit time across the gain medium relative to the roundtrip time lends itself to an active mode-locking scheme in which the gain medium is pumped with picosecond time-scale electrical pulses at the roundtrip frequency. A preliminary simulation based on the Maxwell-Bloch equations suggests that mode-locked light pulses as short as a few picoseconds can be generated by implementing such a synchronous pumping in the ERC-QCL. A complete analysis of this mode-locking scheme will be the object of a following work.

In summary, we have demonstrated an external ring-cavity quantum cascade laser. The laser transitions from bidirectional to directional emission when the current surpasses a critical value. In the latter regime spatial hole burning is suppressed, which leads to a single-mode spectrum, in contrast with the multimode spectrum typical of FP-QCLs. The ERC-QCL is a good platform for mode-locked pulsed operation and for high sensitivity spectroscopic detection.

The authors wish to thank Anish Goyal from MIT Lincoln Laboratory for the anti-reflection coatings and Franz Kärtner for helpful discussions and suggestions. We acknowledge support from the National Science Foundation (NSF) Award No. ECCS-1230477. T.S.M. was supported by an NSF Graduate Student Fellowship. This work was performed in part at the Center for Nanoscale Systems (CNS) at Harvard University, a member of the National Nanotechnology Infrastructure Network (NNIN), which is supported by the NSF.

[1]A. Gordon, C. Y. Wang, L. Diehl, F. X. Kärtner, A. Belyanin, D. Bour, S. Corzine, G. Höfler, H. C. Liu, H. Schneider, T. Maier, M. Troccoli, J. Faist, and F. Capasso, Phys. Rev. A **77**, 053804 (2008).
[2]C. Y. Wang, L. Kuznetsova, V. M. Gkortsas, L. Diehl, F. X. Kärtner, M. A. Belkin, A. Belyanin, X. Li, D. Ham, H. Schneider, P. Grant, C. Y. Song, S. Haffouz, Z. R. Wasilewski, H. C. Liu, and F. Capasso, Opt. Express **17**, 12929–12943 (2009).
[3]V. M. Gkortsas, C. Wang, L. Kuznetsova, L. Diehl, A. Gordon, C. Jirauschek, M. A. Belkin, A. Belyanin, F. Capasso, and F. X. Kärtner, Opt. Express **18**, 13616–13630 (2010).
[4]A. E. Siegman, *Lasers* (University Science Books, Sausalito, CA, 1986), p. 1165.
[5]C. C. Nshii, C. N. Ironside, M. Sorel, T. J. Slight, S. Y. Zhang, D. G. Revin, and J. W. Cockburn, Appl. Phys. Lett. **97**, 231107 (2010).
[6]G. Van der Sande, L. Gelens, P. H. Tassin, A. Scire, and J. Danckaert, J. Phys. B **41**, 095402 (2008).
[7]T. Perez, A. Scire, G. Van der Sande, P. Colet, and C. R. Mirasso, Opt. Express **15**, 12941–12948 (2007).
[8]M. Sorel, G. Giuliani, A. Scire, R. Miglierina, S. Donati, and P. J. R. Laybourn, IEEE J. Quant. Electron. **39**(10), 1187–1195 (2003).
[9]M. Sorel, P. J. R. Laybourn, G. Giuliani, and S. Donati, Appl. Phys. Lett. **80**, 3051 (2002).
[10]M. F. Booth, A. Schremer, and J. M. Ballantyne, Appl. Phys. Lett. **76**, 1095 (2000).
[11]M. Sargent III, Phys. Rev. A **48**, 717–726 (1993).
[12]K. Fujita, S. Furuta, A. Sugiyama, T. Ochiai, T. Edamura, N. Akikusa, M. Yamanishi, and H. Kan, IEEE J. Quantum Electron. **46**, 683–688 (2010).
[13]A. Hugi, R. Terazzi, Y. Bonetti, A. Wittmann, M. Fischer, M. Beck, J. Faist, and E. Gini, Appl. Phys. Lett. **95**, 061103 (2009).
[14]G. Stewart, K. Atherton, and B. Culshaw, Opt. Lett. **29**, 442–444 (2004).
[15]P. V. Pokasov, A. A. Kurbatov, D. Yu. Primakov, E. A. Titov, and S. N. Bagayev, Laser Phys. **15**, 1046–1055 (2005).
[16]V. M. Baev, T. Latz, and P. E. Toschek, Appl. Phys. B **69**, 171 (1999).